

Supplement of Atmos. Chem. Phys., 18, 12315–12327, 2018
<https://doi.org/10.5194/acp-18-12315-2018-supplement>
© Author(s) 2018. This work is distributed under
the Creative Commons Attribution 4.0 License.



Supplement of

Tropospheric sources and sinks of gas-phase acids in the Colorado Front Range

James M. Mattila et al.

Correspondence to: Delphine K. Farmer (delphine.farmer@colostate.edu)

The copyright of individual parts of the supplement might differ from the CC BY 4.0 License.

Supplemental Figures

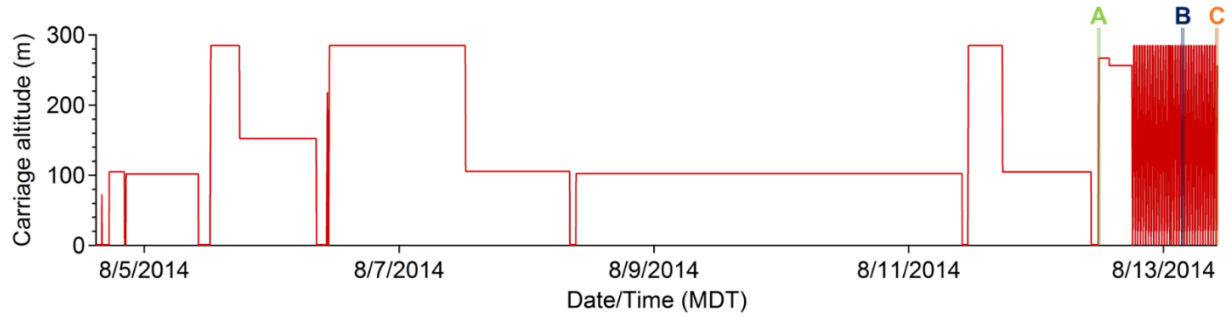


Figure S1. Timeseries of tower elevator carriage altitude throughout the reported measurement period. Representative noon, night, and morning vertical profiles were measured at the periods denoted 'A', 'B', and 'C', respectively.

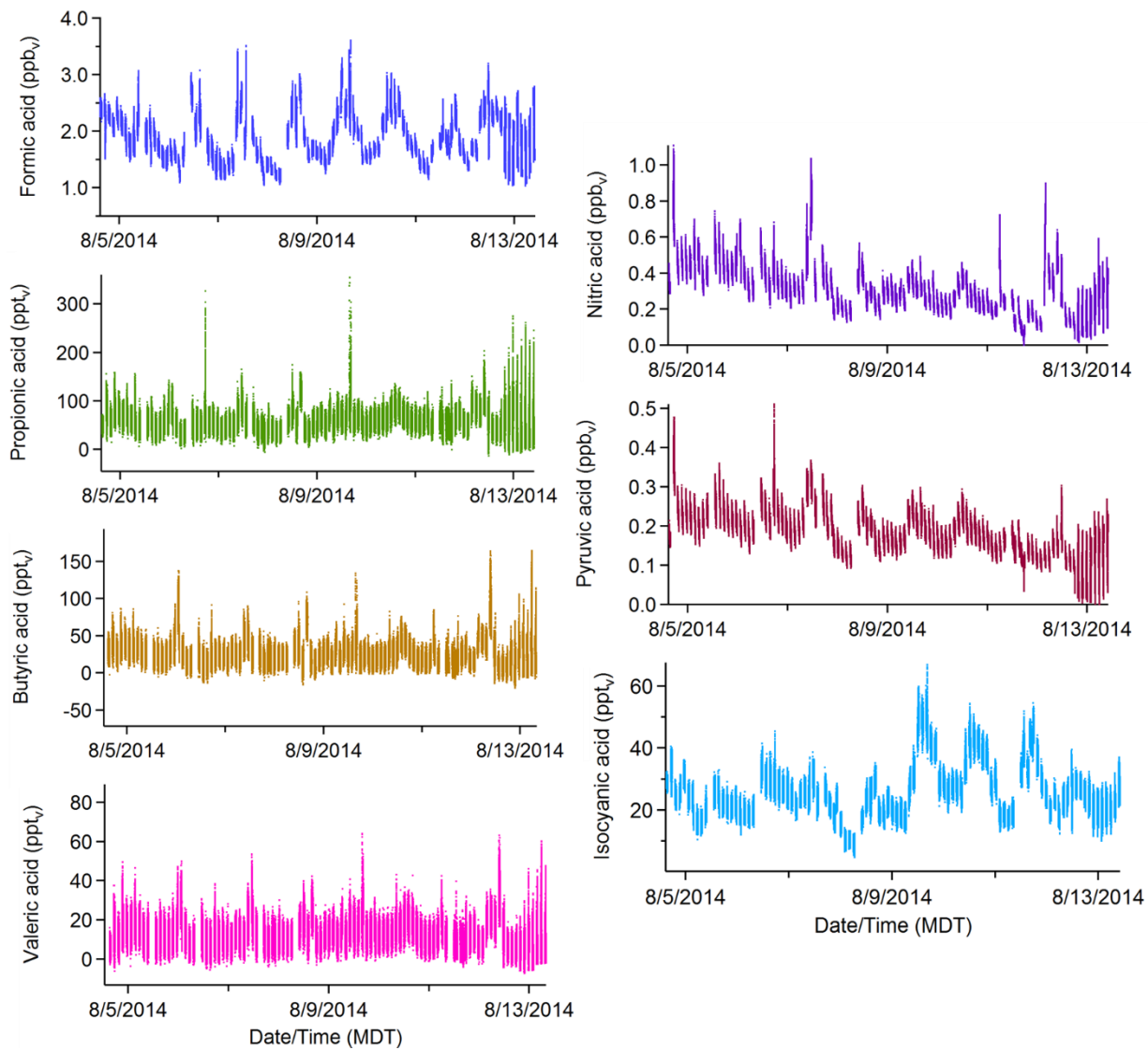


Figure S2. Mixing ratio data timeseries for all detected gas-phase acids spanning the reported data acquisition period. All data were collected at 1 Hz acquisition rates.

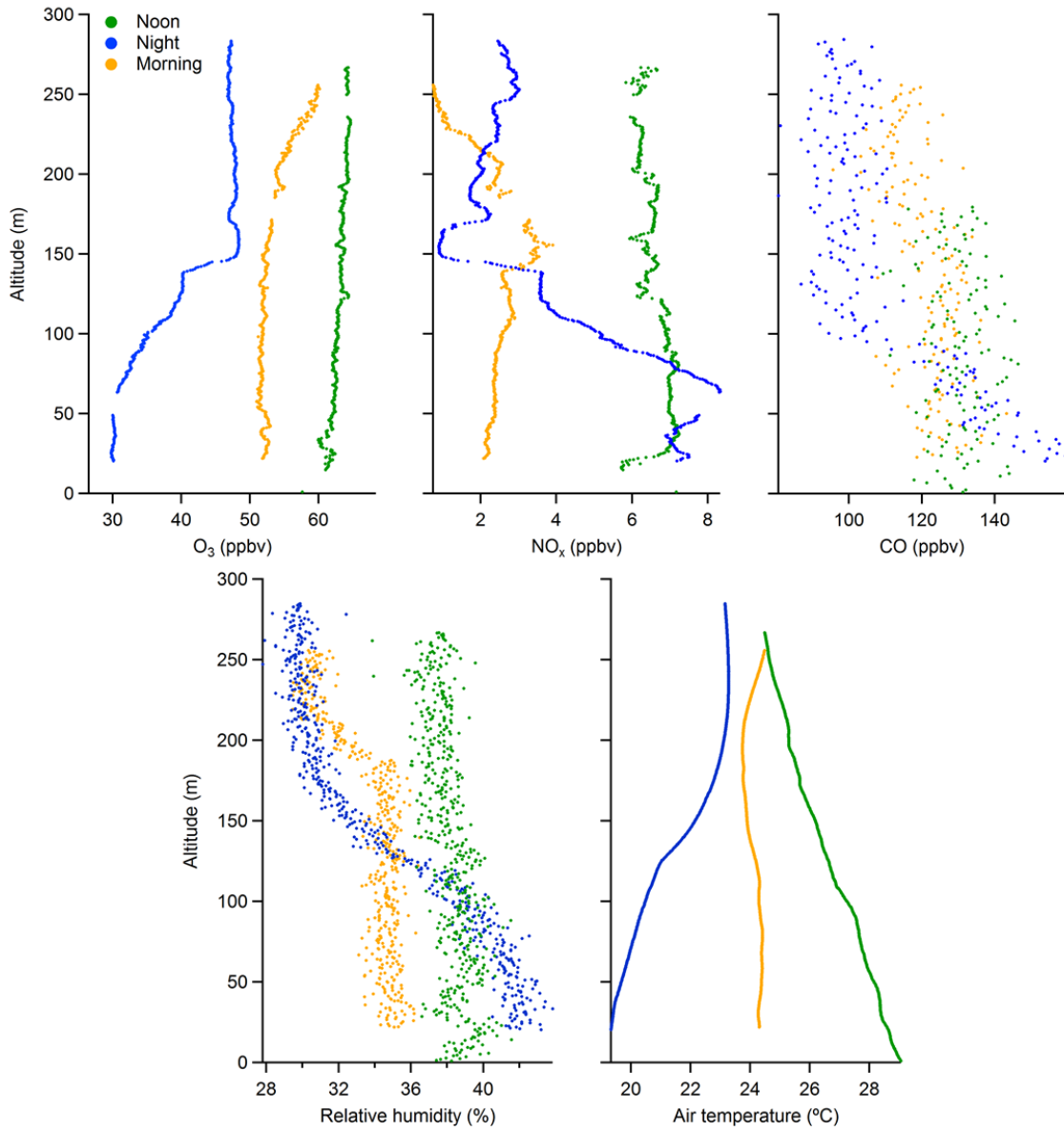


Figure S3. Vertical profiles of O₃, NO_x, CO, relative humidity, and air temperature at representative noon, night, and morning periods.

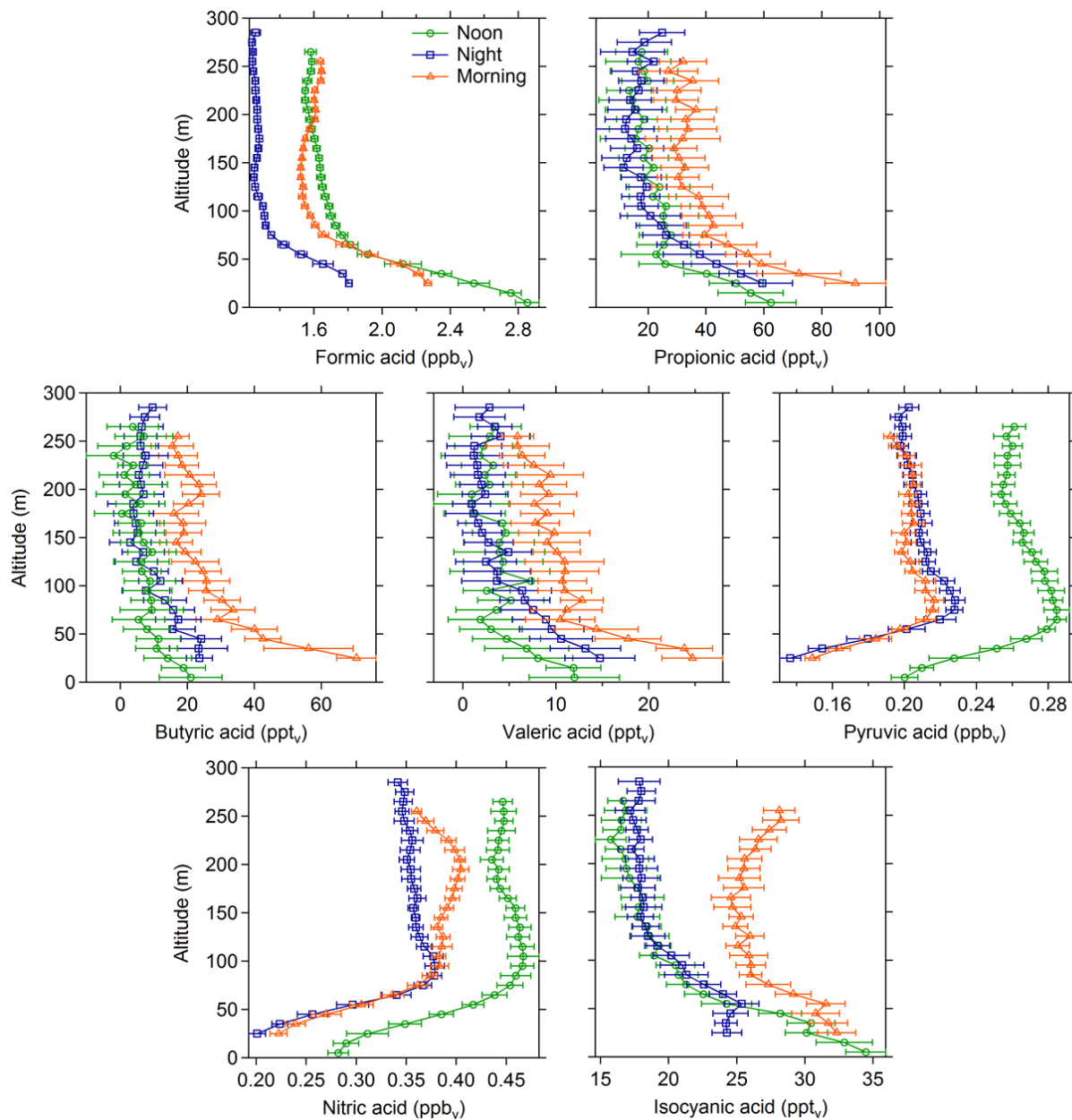


Figure S4. Vertical profiles for all detected gas-phase acids at representative noon, night, and morning periods, showing mixing ratios as a function of altitude. Data are binned by altitude (10 m per bin). Data points are means of each bin. Error bars represent \pm one standard deviation of binned values.

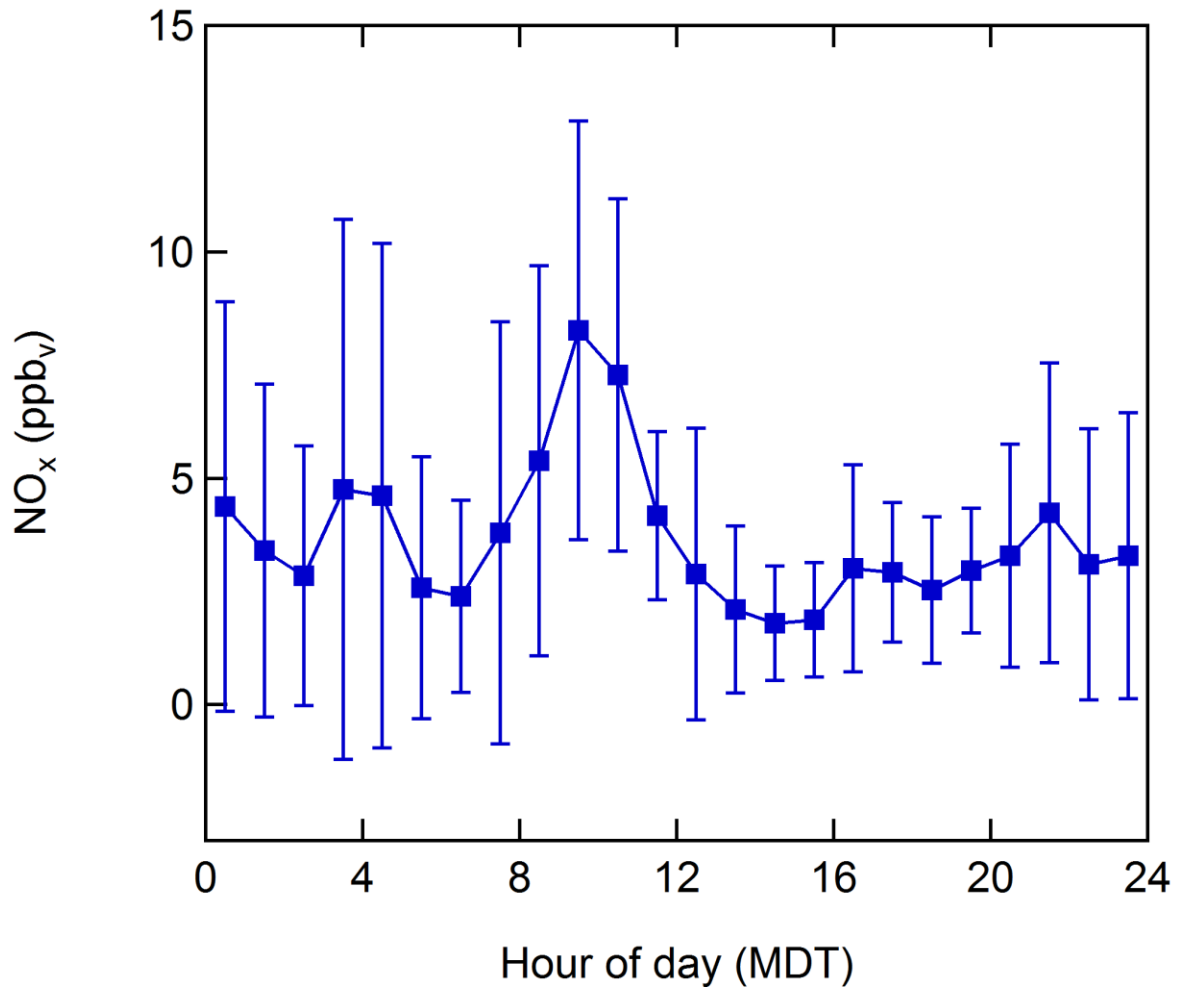


Figure S5. Diel profile of NO_x measured at the site throughout the reported measurement period. Data are binned by hour of day. Data points are binned means, and error bars are ± one standard deviation of binned data.

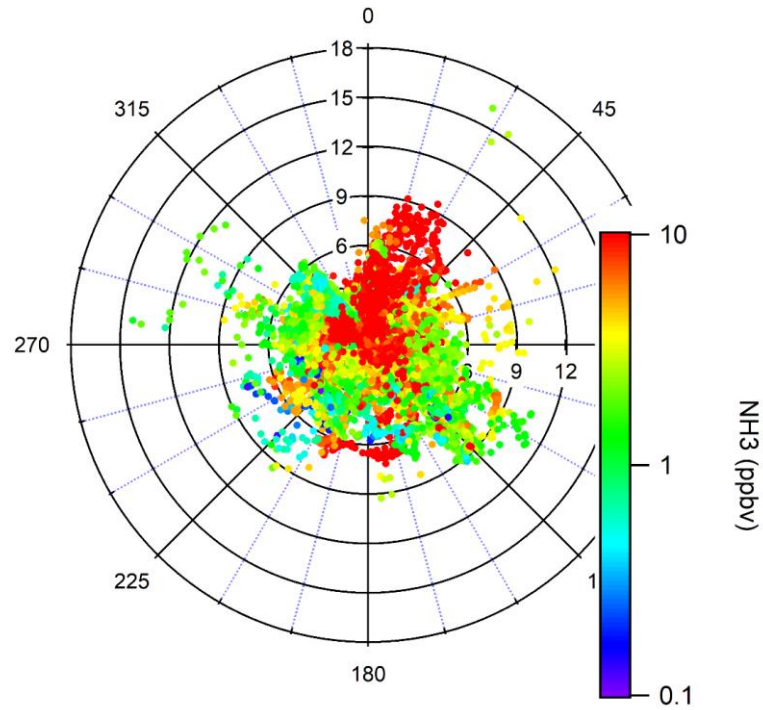


Figure S6. Wind plot of ammonia measured at the BAO tower during the reported measurement period. Data points are colored by mixing ratio. Angular axis corresponds to wind direction (degrees), with 0, 90, 180, and 270 degrees corresponding to N, E, S, and W cardinal directions, respectively. Radial axes correspond to wind speed (m s^{-1}).

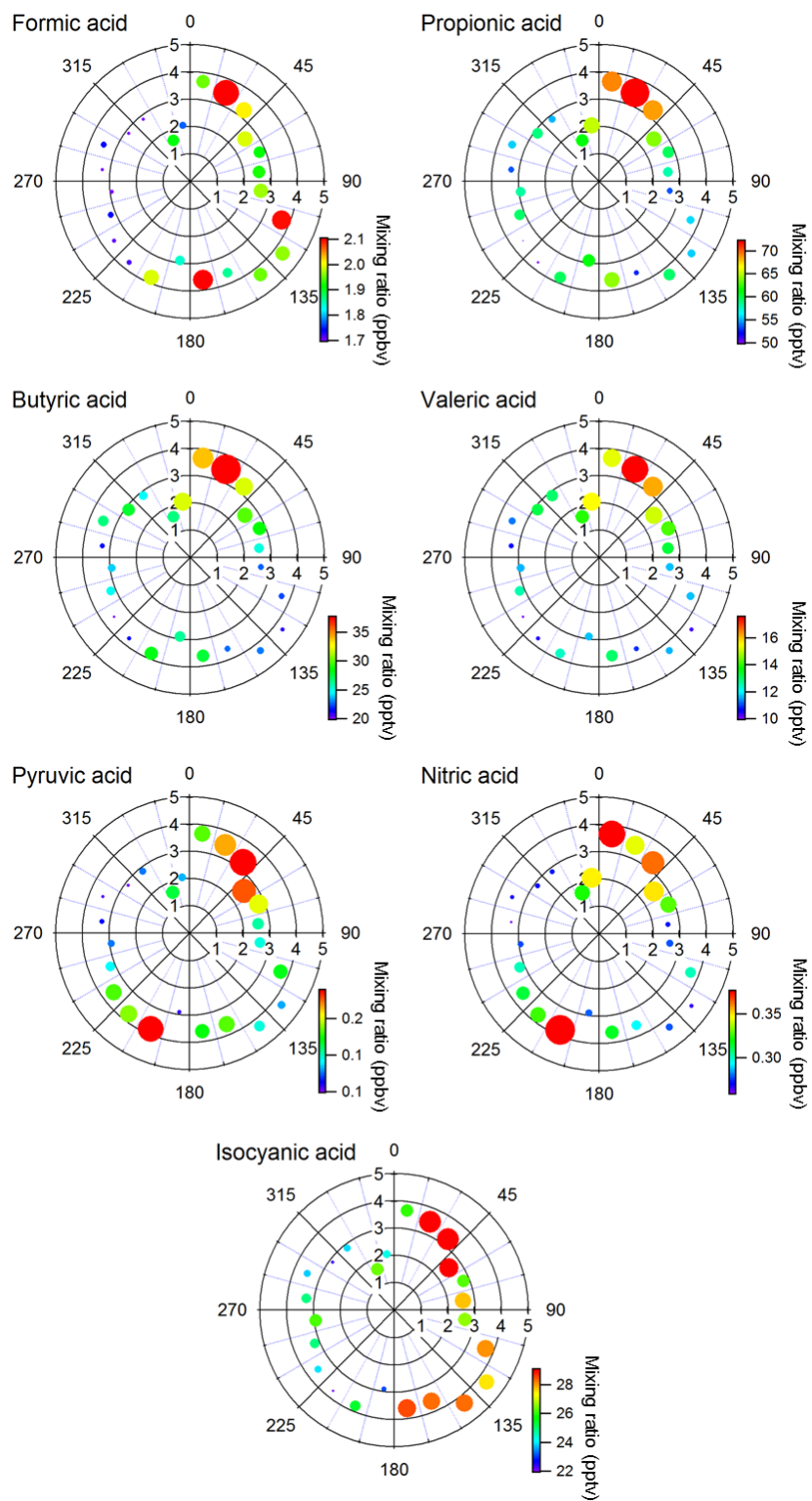


Figure S7. Radial plots with wind speed (m s^{-1}), direction (degrees), and acid mixing ratio data binned into 15° angular bins. Degrees correspond to cardinal directions (i.e. 0° is N, 90° is E, etc.). Radial positions of markers represent the diel average wind speed within each angular bin. Markers are colored and sized by the diel average mixing ratio of each acid within each angular bin.

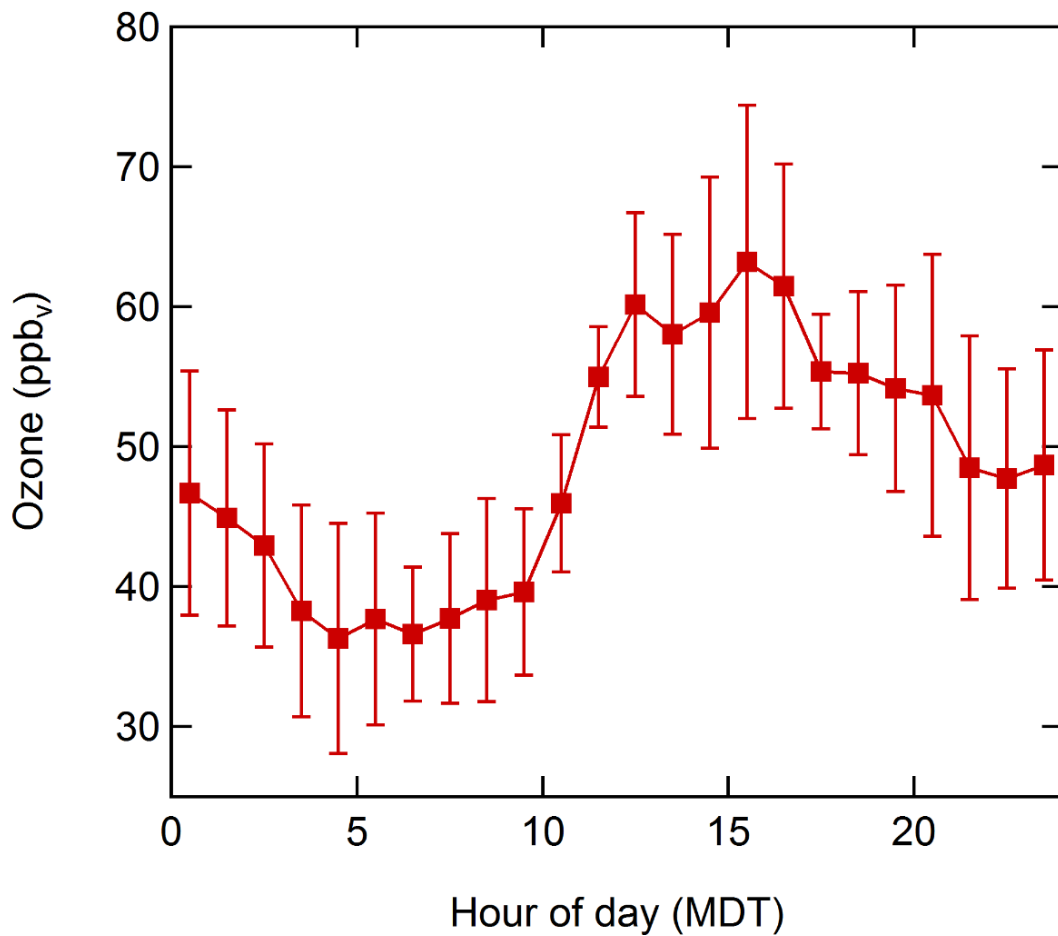


Figure S8. Diel profile of ozone measured at the site throughout the reported measurement period. Data are binned by hour of day. Data points are binned means, and error bars are \pm one standard deviation of binned data.

Supplemental Discussion

In-laboratory gas-phase acid calibrations and FRAPPE sensitivity estimations

The calibration setup shown in Figure S7 was recreated in a laboratory setting, with the heated calibration oven containing permeation standards of all gas-phase acid compounds presented here. External standard calibrations of these compounds were performed to determine ToF-CIMS sensitivities of these compounds. A sensitivity-ratio estimation was employed to estimate instrumental sensitivity of these compounds during the FRAPPE campaign:

$$S_{x,FRAPPE} = \frac{S_{x,lab}}{S_{FA,lab}} S_{FA,FRAPPE}$$

where $S_{x,FRAPPE}$ is the estimated sensitivity of a given gas-phase compound during FRAPPE, $S_{x,lab}$ is the measured sensitivity of a given gas-phase compound from in-lab calibrations, $S_{FA,lab}$ is the measured sensitivity of formic acid from in-lab calibrations, and $S_{FA,FRAPPE}$ is the mean sensitivity of formic acid during FRAPPE. A table of estimated sensitivity values for all gas-phase species measured during FRAPPE is provided below.

| Gas-phase acid | Propionic | Butyric | Valeric | Pyruvic | Nitric | Isocyanic |
|-------------------------------------|-----------|---------|---------|---------|--------|-----------|
| Est. Sensitivity (ncps/ppbv) | 2590 | 4700 | 6300 | 20400 | 24000 | 85900 |

Estimating NH_4NO_3 aerosol formation as sink for HNO_3

Reactions between gas-phase HNO_3 and NH_3 produce NH_4NO_3 aerosol, and therefore act as a potential tropospheric sink for gas-phase HNO_3 . Gas-particle phase partitioning is an equilibrium process that depends on ambient temperature and relative humidity (RH) (Seinfeld and Pandis, 1998; Li et al., 2014). Methods for estimating NH_4NO_3 formation from HNO_3 and NH_3 are outlined by Seinfeld and Pandis (1998). Deliquescence relative humidity (DRH) can be calculated by the following:

$$\ln(DRH) = \frac{723.7}{T} + 1.6954$$

Ambient RH at the site was below the DRH for > 90% data reported here, indicating that most NH_4NO_3 produced was in the solid phase. Neglecting aqueous phase aerosol production allows for a simplified estimation of NH_4NO_3 partitioning (as previously performed by Li et al. (2014)), which can be expressed by the following equilibrium expression:



and the accompanying equilibrium constant is therefore given by:

$$K = [NH_3][HNO_3]$$

where $[\text{NH}_3]$ and $[\text{HNO}_3]$ are the gas-phase mixing ratios of NH_3 and HNO_3 , respectively. The expected equilibrium constant, K_p , is calculated by:

$$\ln(K_p) = 84.6 - \frac{24200}{T} - 6.1 \ln\left(\frac{T}{298}\right)$$

where T is ambient temperature. Solid NH_4NO_3 formation is favorable when $K > K_p$ —i.e. when the system is supersaturated with NH_3 and HNO_3 . $K > K_p$ for < 10% of the data reported here, indicating that NH_4NO_3 formation was predominantly unfavorable, and therefore suggesting that this process does not serve as a major sink of gas-phase HNO_3 . NH_4NO_3 formation is typically less favorable when RH is low and temperature is high (Li et al., 2014), as is the case for a typical summer day in the Front Range.

Estimating aqueous-phase partitioning of gas-phase acids

Aqueous-phase partitioning was evaluated as a potential sink for gas-phase acids by using Henry's Law:

$$H_x = \frac{[X]_{aq}}{P_x}$$

where H_x is the Henry's Law constant for a given gas-phase acid, and $[X]_{aq}$ and P_x are the aqueous concentration and partial pressure of said acid species, respectively. P_x was calculated by gas-phase acid mixing ratio data, as well as meteorological data collected during the campaign. Moles of a given acid in the aqueous-phase was determined by $[X]_{aq}$ and ambient liquid water concentration (LWC). LWC in the Front Range during the summer is estimated to be around $1 \mu\text{g m}^{-3}$, based on continental estimates of LWC reported by Carlton and Turpin (2013). To account for the effects of pH on solubility, $[X]_{aq}$ was calculated as the following:

$$[X]_{aq} = H_x P_x \left(1 + \frac{K_a}{[H^+]}\right)$$

where K_a is the acid dissociation equilibrium constant for a given acid (Levanov et al., 2017; Fischer and Warneck, 1991; Borduas et al., 2016; Smith and Martell, 2004), and $[H^+]$ is the aqueous concentration of hydronium ion. Combining aqueous-phase moles of a given acid with the ideal gas law, and meteorological data from the site yields a total loss of said acid from the gas-phase through partitioning. Total loss of each acid calculated at various atmospherically-relevant pH values are reported below. This estimation is limited in that it neglects the effects of other dissolved ions on solubility, though we would not expect a change of several orders of magnitude by accounting for these effects.

| | Loss via aqueous partitioning (ppbv) | | | | | | |
|-----------|---|------------------|----------------|----------------|----------------|---------------|------------------|
| pH | Formic | Propionic | Butyric | Valeric | Pyruvic | Nitric | Isocyanic |
| 2 | 1.4E-10 | 1.4E-10 | 1.1E-10 | 5.4E-11 | 1.5E-08 | 1.8E-05 | 1.4E-10 |
| 3 | 1.6E-10 | 1.4E-10 | 1.2E-10 | 5.4E-11 | 8.3E-08 | 1.8E-04 | 1.6E-10 |
| 4 | 3.8E-10 | 1.6E-10 | 1.3E-10 | 6.1E-11 | 7.6E-07 | 1.8E-03 | 4.2E-10 |
| 5 | 2.5E-09 | 3.2E-10 | 2.9E-10 | 1.3E-10 | 7.6E-06 | 1.8E-02 | 2.9E-09 |
| 6 | 2.4E-08 | 1.9E-09 | 1.8E-09 | 8.0E-10 | 7.6E-05 | 1.8E-01 | 2.8E-08 |

Supplemental References

Borduas, N., Place, B., Wentworth, G., Abbatt, J., and Murphy, J.: Solubility and reactivity of HNCO in water: insights into HNCO's fate in the atmosphere, 16, 703-714, 2016.

Carlton, A. G., and Turpin, B. J.: Particle partitioning potential of organic compounds is highest in the Eastern US and driven by anthropogenic water, *Atmos. Chem. Phys.*, 13, 10203-10214, doi:10.5194/acp-13-10203-2013, 2013.

Fischer, M., and Warneck, P.: The dissociation constant of pyruvic acid: determination by spectrophotometric measurements, 95, 523-527, 1991.

Levanov, A., Isaikina, O. Y., and Lunin, V.: Dissociation constant of nitric acid, 91, 1221-1228, 2017.

Li, Y., Schwandner, F. M., Sewell, H. J., Zivkovich, A., Tigges, M., Raja, S., Holcomb, S., Molenaar, J. V., Sherman, L., Archuleta, C., Lee, T., and Collett, J. L.: Observations of ammonia, nitric acid, and fine particles in a rural gas production region, *Atmos. Environ.*, 83, 80-89, doi:10.1016/j.atmosenv.2013.10.007, 2014.

Seinfeld, J. H., and Pandis, S. N.: *Atmospheric Chemistry and Physics*, 1 ed., Wiley-Interscience, Canada, 1998.

Smith, R. M., and Martell, A. E.: NIST Standard Reference Database 46, in, 2004.